Ecological Informatics 89 (2025) 103168

Contents lists available at ScienceDirect

Ecological Informatics

journal homepage: www.elsevier.com/locate/ecolinf

A multi-level, multi-scale comparison of LiDAR- and LANDSAT-based habitat selection models of Mexican spotted owls in a post-fire landscape

Ho Yi Wan[a,b,*], Michael A. Lommler[c,d], Samuel A. Cushman[c,e], Jamie S. Sanderlin[f], Joseph L. Ganey[g,1], Andrew J. Sánchez Meador[c,h], Paul Beier[i]

[a] Department of Wildlife, California State Polytechnic University Humboldt, 1 Harpst Street, Arcata, CA 95521, USA
[b] Department of Wildlife Ecology and Conservation, University of Florida, Gainesville, FL 32611, USA
[c] School of Forestry, Northern Arizona University, Flagstaff, AZ 86011, USA
[d] Bureau of Land Management, Colorado State Office, Lakewood, CO 80215, USA
[e] University of Oxford, Department of Biology, Oxford, UK
[f] USDA Forest Service, Rocky Mountain Research Station, Flagstaff, AZ, USA
[g] USDA Forest Service, Rocky Mountain Research Station, Flagstaff, AZ, USA
[h] Ecological Restoration Institute, Northern Arizona University, Flagstaff, AZ 86011, USA
[i] Center for Large Landscape Conservation, Bozeman, MT 59715, USA

A R T I C L E I N F O

Keywords:
Habitat suitability
Megafire
Scaling
Habitat suitability model
Strix occidentalis
Wildfire

A B S T R A C T

The increasing frequency and severity of wildfires pose significant challenges for habitat conservation, particularly in post-fire landscapes. This study evaluates the habitat selection of the Mexican spotted owl (*Strix occidentalis lucida*) in a post-fire environment using multi-level and multi-scale models derived from LANDSAT and LiDAR data. By focusing on 2nd order (home range selection) and 3rd order (microhabitat selection) habitat use, we assessed the predictive performance and ecological relevance of these datasets. Optimizing predictors across spatial scales revealed that large trees, high canopy cover, and mixed-conifer forests were consistently critical for habitat selection, regardless of the data source. When optimized for spatial scale, LANDSAT- and LiDAR-based models exhibited comparable predictive accuracy (AUC = 0.976 and 0.975, respectively), emphasizing the critical role of scale in model performance. Both models had low out-of-bag (OOB) error rates (0.037 for LANDSAT and 0.050 for LiDAR), indicating high classification reliability. High-severity fire burned 36.6 % of the study area, negatively impacting owl habitat at fine scales around nest and roost sites, whereas a mosaic of burned and unburned patches provided foraging opportunities. Spatial disagreement analysis revealed notable differences in predicted habitat suitability between LANDSAT and LiDAR models, particularly in areas with complex topography and forest composition. These findings underscore the complementary strengths of both datasets, with LiDAR excelling in fine-scale structural detail and LANDSAT providing broad-scale compositional insights. Integrating these technologies offers a scalable and cost-effective framework for monitoring habitat recovery and guiding conservation strategies in fire-affected landscapes.

1. Introduction

In recent years, large wildfires have increasingly devastated human communities and ecosystems with greater frequency and severity (Higuera, 2015). These wildfires have destroyed towns, disrupted livelihoods, and caused extensive habitat loss, displacing wildlife populations (Balch et al., 2024; Driscoll et al., 2021). The increasing occurrence of "mega-fires" (i.e., fires >10,000 ha to >100,000 ha) is largely attributed to a combination of climate change, land-use and fire management practices, and human expansion into wildlands (Balch et al., 2017; Collins et al., 2021; Jones et al., 2022; Stephens et al., 2014). Although wildfires are a natural part of many ecosystems, recent fires have introduced disturbance regimes to which ecosystems may not be historically adapted (Hagmann et al., 2021). As these trends continue, understanding how wildfire impacts forest structure and composition has become a pressing concern for land managers.

* Corresponding author at: Department of Wildlife, California State Polytechnic University Humboldt, 1 Harpst Street, Arcata, CA 95521, USA.
E-mail address: hw83@humboldt.edu (H.Y. Wan).
[1] Retired.

https://doi.org/10.1016/j.ecoinf.2025.103168
Received 13 February 2025; Received in revised form 26 April 2025; Accepted 27 April 2025
Available online 28 April 2025

Past research has shown that habitat suitability models developed using remotely sensed data can improve our understanding of wildfire risks and impacts on habitats (Hysen et al., 2023; Khosravi et al., 2022; Wan et al., 2020). These models quantify species-environment relationships, offering critical insights into how wildfires transform habitat conditions across landscapes, and can assess these relationships at multiple spatial scales (Wan et al., 2020). However, the accuracy and performance of these models are strongly influenced by the quality and resolution of the input data. Historically, many habitat and connectivity models have relied on LANDSAT satellite imagery to capture forest structure and vegetation conditions (Timm et al., 2016; Wan et al., 2017, 2019a). LANDSAT data has several advantages: it is freely available, offers long-term temporal coverage, and provides a reasonable spatial resolution (30-m pixel) suitable for large-scale ecological studies.

More recently, LiDAR (Light Detection and Ranging) technology has emerged as a powerful alternative to LANDSAT for capturing forest structure. LiDAR provides highly detailed three-dimensional data on vegetation structure at finer resolutions (≤10-m), making it possible to map forest canopy height, density, and understory conditions more precisely than LANDSAT (Hummel et al., 2011). LiDAR has been shown to produce more accurate characterizations of forest composition and structure than traditional satellite imagery, especially in heterogeneous landscapes (Blackburn et al., 2021). However, LiDAR also has notable limitations compared to satellite remote sensing, including high acquisition costs, limited spatial coverage, and infrequent temporal updates (Ackers et al., 2015). While recent advances in computing power and sensor technology have improved the accessibility of LiDAR data (Vierling et al., 2008), its use still demands extensive preprocessing overheads, such as filtering ground returns, correcting sensor errors, and converting to higher-level products.

Because forest structure is closely linked to habitat potential, LiDAR offers an opportunity to improve models of post-fire habitat conditions. However, few studies have directly compared the performance of LiDAR- and LANDSAT-derived habitat suitability models in post-fire landscapes (Galbraith et al., 2024; Moran et al., 2020). Here, we conducted a post-fire assessment of habitat use with the primary goal of comparing the effectiveness of LiDAR and LANDSAT data for modeling habitat selection. Our study focused on the 2002 Rodeo-Chediski Fire in central Arizona, which burned 187,000 ha, with 36.6 % of the area classified as high-severity burn by Monitoring Trends in Burn Severity (Monitoring Trends in Burn Severity [MTBS], 2025). This fire footprint provided a landscape to assess Mexican spotted owl (*Strix occidentalis lucida*) habitat selection 13–15 years after burning. By doing so, we evaluated both the long-term persistence of owl habitat after severe wildfire and the relative strengths of different remote sensing approaches for capturing key habitat features.

The Mexican spotted owl is a federally listed Threatened species that occupies mixed-conifer and pine-oak (*Pinus* spp. – *Quercus* spp.) forests, habitats that have been heavily impacted by large, high-severity wildfires in the southwestern United States (Ganey et al., 2017; Wan et al., 2018). The owl is particularly sensitive to changes in forest structure, as it prefers dense canopy cover for nesting and roosting, while also utilizing early seral patches for foraging (Roberts et al., 2011). Previously, Kramer et al. (2021) used LiDAR to study elevational differences in nocturnal habitat selection by spotted owls and highlighted the species' reliance on forest structures. This reliance on specific forest structures makes the species an ideal candidate for evaluating how well LiDAR and LANDSAT data capture post-fire habitat characteristics. Furthermore, because the owl exhibits strong site fidelity and has long life spans (Gutiérrez et al., 1995), its habitat preferences remain relatively stable over time, providing a clear test case for long-term habitat selection analysis. By focusing on the Mexican spotted owl, we can assess the performance of these two remote sensing technologies in mapping critical forest habitats that are essential for both conservation efforts and wildfire management.

In addition, we conducted this study at multiple levels of habitat selection, specifically the 2nd order of selection (hereafter, home range level) and 3rd order of selection (hereafter, microhabitat level) (Johnson, 1980). By evaluating both levels, we can better understand post-fire habitat conditions associated with Mexican spotted owls across scales, offering valuable knowledge given that most previous models focus on unburned landscapes (Nayeri et al., 2024; Timm et al., 2016; Wan et al., 2017, 2019a). This multi-level approach is useful because species often exhibit different preferences at broader versus finer scales, and the impacts of fire on habitat availability and suitability may vary accordingly. Examining habitat selection at both levels allows us to capture this scale-dependent variation, providing more nuanced insights into how well LiDAR and LANDSAT data represent habitat changes across different spatial extents. This, in turn, helps land managers develop more effective conservation and wildfire management strategies that are sensitive to the varying needs of wildlife across scales.

We hypothesized that LiDAR-based models would outperform LANDSAT-based models in predicting habitat suitability, particularly in landscapes affected by severe wildfire due to their finer resolution in depicting forest structures. Additionally, we examined whether the characteristic spatial scales of forest structure metrics and the spatial prediction differed between the best models produced by the two datasets. We hypothesized that LiDAR-based models would tend to select finer scales than LANDSAT-based models due to the differences in the spatial information density of these two data sources. By incorporating both LiDAR and LANDSAT data, we aimed to evaluate how advancements in remote sensing technology can enhance our understanding of wildfire impacts on forest ecosystems. This comparison can inform future efforts to manage post-fire landscapes more effectively by providing more precise tools for identifying remnant habitat for species dependent on mature forests.

2. Methods

2.1. Study area

Our study area encompassed 18,800 ha within the Rodeo-Chediski fire perimeter, located about 8 km southwest of Heber-Overgaard, AZ. Bounded by Arizona State Highway 260 to the north, Forest Service Road 512 to the west, and the Fort Apache Indian Reservation to the south (Fig. 1). This region includes all known Mexican spotted owl habitats within the fire's scope. Approximately 14,700 ha lie in the Black Mesa Ranger District of the Apache-Sitgreaves National Forest, with the remaining 4100 ha in the Pleasant Valley Ranger District of the Tonto National Forest. Dominated by the Mogollon Rim, elevation ranges from 1890 m in Canyon Creek to 2350 m on the Rim, with deep canyons carved into the Rim's southern face. Vegetation was dominated by ponderosa pine (*Pinus ponderosa*) forests, covering 66.2 % of the

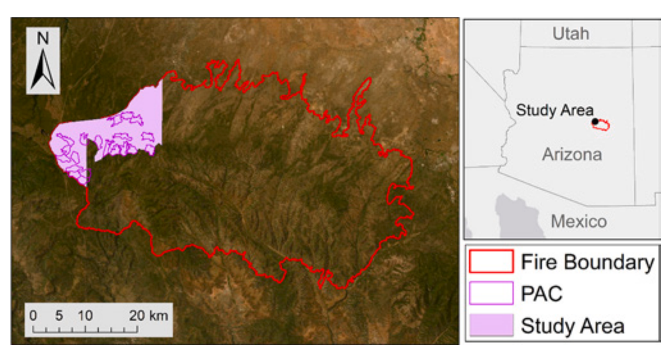

Fig. 1. Map of the 2002 Rodeo-Chediski fire area in east-central Arizona and the included 18,800 ha study area on the Apache-Sitgreaves and Tonto National Forests, adjacent to the Fort Apache Indian Reservation. Also shown are the boundaries of 20 Mexican spotted owl Protected Activity Centers (PACs) designated before the fire.

landscape. Mixed-conifer and pine-oak forests interspersed across canyons and steep north-facing slopes. Mixed-conifer forests are characterized by a combination of ponderosa pine, Douglas-fir (*Pseudotsuga menziesii*; 0.2 %), and white fir (*Abies concolor*; 0.1 %), while pine-oak forests primarily consist of ponderosa pine and Gambel oak (*Quercus gambelii*; 9.3 %). Pinyon-juniper woodlands, which covers 8.4 % of the area are also common and include pinyon pine (*Pinus* spp.) and juniper (*Juniperus* spp.) species. Many post-fire areas have regenerated into shrubby thickets (e.g., *Arctostaphylos pungens*, *A. pringlei*) or grasslands (e.g., *Bouteloua gracilis*, *Festuca arizonica*). Our study area contained 20 designated Mexican spotted owl Protected Activity Centers (PACs) as defined in the Final Recovery Plan (U.S. Fish and Wildlife Service, 2012) before the fire. However, the number of PACs occupied immediately before the fire is uncertain. One additional PAC was established in 2014, based on owl locations developed during this study. We defined the study landscape area for home range selection based on the 21 known Protected Activity Centers (PACs), which represent established territories for Mexican spotted owls.

According to MTBS classification, which utilizes the Relativized differenced Normalized Burn Ratio (RdNBR) and the Composite Burn Index (CBI) to assess burn severity, approximately 23 % and 21 % of the area experienced high- and moderate-severity burns, respectively (Monitoring Trends in Burn Severity [MTBS], 2025). Salvage logging impacted 1632 ha (~8.6 %) of the study area, including 65 ha within five PACs. Additionally, 613 ha (~3.3 %) were re-burned at low severity in May of 2012 by the Bull Flat fire (Monitoring Trends in Burn Severity [MTBS], 2025), an aspect disregarded in this analysis.

2.2. Spotted owl surveys

During the 2014–2016 breeding seasons, we surveyed spotted owls primarily using the nocturnal acoustic protocol in which surveyors project spotted owl calls and listen for responses at call points (Forsman, 1983). We established a network of 602 call points within 212 grid cells (100-ha each) to completely survey the study area. We surveyed each call point >4 times each year (spending 10 min at each point) during the April to August portion of the breeding season. Because acoustic surveys usually yield imprecise locations, we followed these detections with diurnal nest and roost surveys, commonly known as "walk-in" surveys.

2.3. Presence/pseudoabsence data

We recorded 134 precise owl locations using Garmin 62S GPS units, with 104 obtained during walk-in surveys and 30 from nocturnal surveys. We excluded nocturnal "fly-in" detections to focus on nesting and roosting sites, leaving 87 unique presence points. For home range habitat selection, we generated 314 pseudoabsence points spatial randomly distributed across the study area. This number was based on an approximate 1:4 presence-to-absence, after which we removed points that were within 1000 m of known presence locations. For microhabitat selection, we generated 87 pseudoabsence points (i.e., paired design for balanced data) randomly drawn from within the 21 PACs to reflect post-fire available habitat within these areas.

2.4. Remote-sensing data and habitat covariates

We acquired airborne LiDAR data for the study area from the Four Forests Restoration Initiative (4FRI). LiDAR acquisition for the area was performed August–September 2013 and June–October 2014 by Quantum Spatial Inc. (additional details provided in Tenneson et al., 2018). The acquisitions were flown during leaf-on conditions (i.e., June to September). Average pulse densities were ≥ 8 pulses·m–2, and vertical accuracies were within 15 cm for each acquisition. As a result, each acquisition falls within the US Geological Survey-defined quality level one (QL1) for lidar data (Heidemann, 2012). The lidar data were processed using the lidR (v. 2.0.3; Roussel et al., 2020; Roussel and Auty, 2023) package in R, employing the Li et al. (2012) algorithm for individual tree segmentation with default parameters. A 1-m digital elevation model (DEM) was generated by filtering for ground-classified points and rasterizing the point cloud using Inverse Distance Weighting (IDW), then summarizing the elevation (mean) for each 1-m pixel. This DEM was used to normalize the point cloud by subtracting each point's elevation from the corresponding DEM elevation directly beneath it. Points were classified as live or dead following the methods of Wing et al. (2015), and individual trees were assigned unique tree IDs using the Li et al. (2012) algorithm with default settings. For each tree, the maximum height point was identified and assigned as the tree's height, which was then used to predict diameter at breast height (DBH) using a power function fit on individual trees (n = 17,137) from stand exams in the surrounding landscape (see Tenneson et al., 2018; Blackburn et al., 2021 for details on data utilized). The resulting equation (Fig. 2) was a power function fit using maximum likelihood, with a pseudo R^2 of 0.711 and a standard error of 7.64 cm. Once these diameter values were obtained, individual trees (both live and dead) were tallied within a 10-m pixel using the following diameter and height thresholds: DBH of ≥30 cm, ≥46 cm, and ≥ 60 cm, and a height threshold of ≥20 m for large trees. Additionally, canopy cover was stratified into two height classes: 2 to 16 m and above 16 m. We calculated percent cover for all live and dead trees, tree density per pixel, and individual tree diameters were converted to basal area, which was summed within the 10-m pixels to estimate live and dead basal area across diameter and height thresholds. The LiDAR picked up three power lines crossing the study area as lines of large trees. We filtered the power lines from the LiDAR data by constructing a buffer around them in ArcGIS 10.6 (Environmental Systems Research Institute [ESRI], 2017) and re-coding the values of the pixels overlaid by the buffer.

We acquired LANDSAT-derived data for basal area, quadratic mean tree diameter, and tree height for this study area from S.E. Sesnie. The creation of these products is described in Dickson et al. (2014). LANDSAT-derived canopy cover was acquired from the National Land Cover Database (Homer et al., 2015). We derived forest composition from the 2014 LANDFIRE Existing Vegetation Type (EVT) layer (LANDFIRE, 2018), and acquired percent canopy cover from the 2011 NLCD dataset (National Land Cover Dataset [NLCD], 2011).

Because the LiDAR and LANDSAT data were collected approximately 12 years after the Rodeo-Chediski Fire and near the time of owl surveys, they represent long-term post-fire vegetation structure, providing a meaningful basis for assessing habitat selection in a recovering landscape rather than capturing only immediate burn effects.

For both LiDAR- and LANDSAT-based approaches, we selected a priori covariates to represent the influence of forest composition, forest structure, fire, and topography upon presence of Mexican spotted owls. We used LiDAR data from 2013 and 2014 to remotely sense vegetation structure and the underlying land surface. LiDAR also allowed us to directly characterize vertical habitat structure (North et al., 2017; Seavy et al., 2009; Vierling et al., 2008) and identify individual large trees and snags (Garcia-Feced et al., 2011). The LiDAR-derived covariates of forest structure measured basal area (BA) of large trees (i.e., BA from trees ≥30, 46, or 60-cm diameter at breast height [DBH]), canopy cover (CC, from 2 to 16-m, and above 16-m), and the number of large trees above several thresholds of DBH (≥ 30, 46, or 60-cm) and height (20-m). We chose thresholds of BA to reflect desired habitat conditions listed in the Mexican spotted owl recovery plan (U.S. Fish and Wildlife Service, 2012) and the upper limits of tree diameter observed on our study area. We assessed CC at two strata to reflect that spotted owls may avoid high CC in the lower strata while selecting for it in taller strata (North et al., 2017). We chose 20-m as a height threshold for large trees because every nest tree we measured on the study area was >20-m height. We calculated slope (in degrees) from our LiDAR-based DEM using the DEM Surface Tools (Jenness, 2013) toolset in ArcGIS, using Horn's method (Horn, 1981). All LiDAR-based rasters used a 10-m pixel size.

For forest composition and fire-related covariates in LiDAR-based

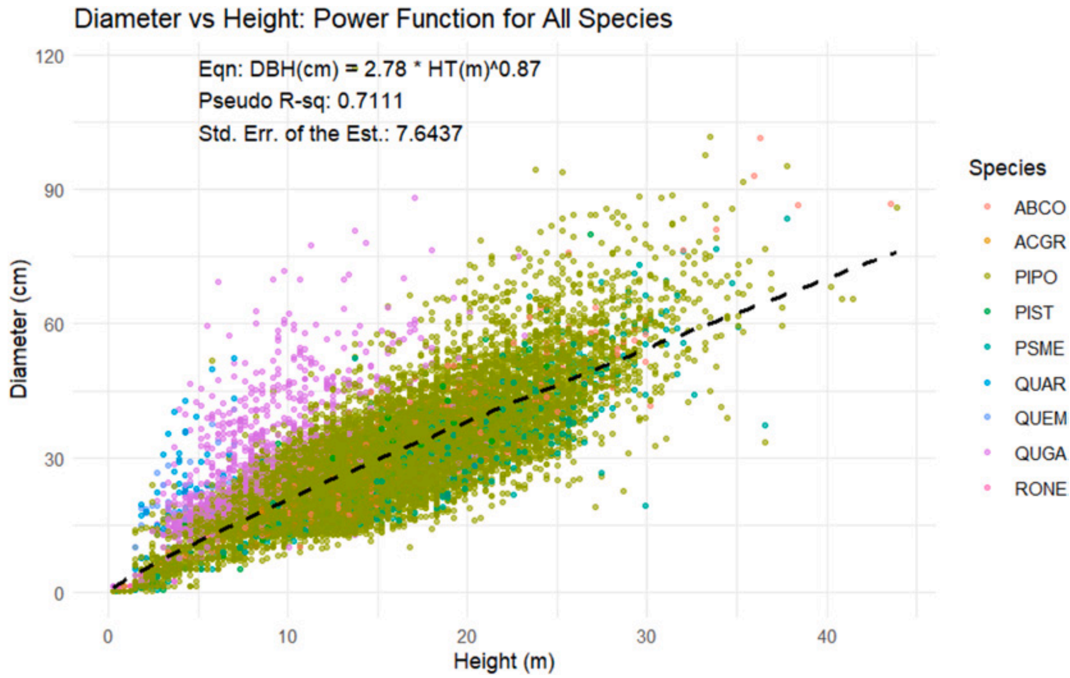

Fig. 2. Diameter at breast height (DBH) as a function of tree height for all species, derived from LiDAR-based tree segmentation. The function was fit using maximum likelihood estimation on 17,137 trees from stand exams in the study area. Colored points represent different tree species, and the dashed line denotes the fitted relationship between height and DBH.

models, we used LANDSAT products based on a 30-m pixel and resampled to a 10-m pixel to match the LiDAR data. We derived two forest composition predictors (proportion of dry and mesic mixed-conifer forest cover) from the LANDFIRE Existing Vegetation Type (EVT) layer (LANDFIRE, 2018). We used three predictors to measure the influence of fire and post-fire logging. Relative delta Normalized Burn Ratio (RdNBR, Miller and Thode, 2007) provides consistent severity measurements across fires and greater accuracy in measuring the high-severity fire class. RdNBR values from 643 to 698 have been estimated to represent the lower threshold of the high-severity fire class in the southwestern U.S. (Dillon et al., 2011; Holden et al., 2009; Singleton et al., 2019). The high-severity fire covariate measured the proportion (0.0–1.00) of the area burned at high severity around each point, which is the most common method of representing fire effects in studies of spotted owls. The proportion salvage logged (0.0–1.00), was acquired from GIS databases for the Apache-Sitgreaves National Forests (U.S. Forest Service, 2018a) and Tonto National Forest (U.S. Forest Service, 2018b).

We used the same forest composition and fire-related covariates for LANDSAT-based models as in LiDAR models. LANDSAT pixels were originally 30-m but resampled to 10-m to match LiDAR pixel size. We used LANDSAT-derived estimates of mean BA, mean canopy cover, mean tree height, and quadratic mean tree diameter to represent forest structure. Unlike LiDAR, this data could not account for individual large trees. We used the National Elevation Database (U.S. Geological Survey, 2014) for topography and calculating slope using DEM surface tools (Jenness, 2013). We calculated mean values at each spatial scale using the Focal Statistics and Extraction tools in ArcGIS for both model types.

2.5. *Univariate scaling*

We ran univariate models across multiple scales for each covariate to identify the optimized scale at which each covariate had the strongest predictive relationship with the presence of spotted owls (sensu McGarigal et al., 2016), which has recently been shown to be a robust method of multi-scale optimization in species-distribution modeling (Cushman et al., 2024). For home range selection models we modeled each covariate separately at scales from radius 100-m to 5000-m in increments of 100-m. For microhabitat selection models we used the 100-m to 1000-m scales. For all covariate scaling we used the R package randomForest (Breiman and Cutler, 2011). We compared model performance using out-of-bag (OOB) error rates.

2.6. *Habitat selection modeling*

Before running multivariate models, we assessed multicollinearity among predictors using pairwise Pearson's correlations for both LANDSAT- and LiDAR-based models for both home range and microhabitat selections (Figs. S1–S4). We considered variables with $|r| \geq 0.7$ to be highly correlated and retained only the most informative predictor (i.e., the one with the lowest OOB error). All variables used in multivariate models were included at their optimal scale as identified in the univariate scaling analysis (above).

All models were run across 2000 decision trees using 3 ($\sqrt{p}$) predictors at each split in each tree (Breiman and Cutler, 2011). We determined the number of trees through an iterative approach, testing 500, 1000, and 2000 trees. While 500 showed instability, 1000 began to stabilize the error rate, and 2000 produced consistent results. We evaluated variable importance using the mean percent decrease in classification accuracy when the value of each variable is randomly permuted. We estimated classification accuracy using the OOB error rate for observations that were not used in construction of a given tree, averaged across all trees.

2.7. *Spatial agreement*

In addition to comparing the optimized spatial scales, model performances, and covariates, we conducted a spatial agreement analysis to evaluate the consistency in habitat suitability predictions between the LiDAR- and LANDSAT-derived models. This was achieved by calculating the absolute difference between the two models using the following equation:

2.8. $|HS_{LiDAR} - HS_{LANDSAT}|$

where HS represents the predicted habitat suitability. A value of 1 indicates complete disagreement between the models, while a value of 0 represents complete agreement. This analysis provides a quantitative measure of how the two models similarly predict habitat suitability across the landscape.

3. Results

3.1. Optimized scales

The optimized scales at which habitat covariates were most strongly associated with the presence of Mexican spotted owls' nests varied between LiDAR- and LANDSAT-based models and across home range and microhabitat habitat selection, highlighting differences in how each dataset captures ecological patterns (Tables 1 and 2).

Optimized scales varied between home range and microhabitat selection for LANDSAT-based models. In home range selection models, variables primarily optimized at intermediate to broader scales. Key predictors, such as CC, HGT, and QMD, showed the highest predictive power at scales of 1700 m, 3800 m, and 4300 m, respectively. Fire-related variables, such as RdNBR and HSF, optimized at broad scales of 5000 m and 4600 m, respectively. MMC and DMC optimized at scales

Table 1
Predictor variables and their optimized scales for multi-scale analysis in LANDSAT-focused models. The optimal scale represents the radius at which each variable exhibited the strongest relationship with the presence of Mexican spotted owls, as determined by out-of-bag error rates. Mean values are based on a 10-m pixel size. The year column indicates when data were collected. Variables included in the final model are marked in the optimal scale column with an asterisk (*).

Predictor	Units and definition	Source (year)	Optimal Scales (m)	
			Home range (2nd order)	Microhabitat (3rd order)
BA	Mean basal area in m^2/ha (all trees)	Sesnie et al. (2006)[1]	2200	100*
CC	Percent canopy cover	National Land Cover Dataset [NLCD] (2011)[2]	1700*	500*
DMC	Proportion dry mixed-conifer forest cover	LANDFIRE (2018)[3]	3100*	900*
HGT	Mean tree height in m	Sesnie et al. (2006)[1]	3800	600
HSF	Percent area burned at high severity	Monitoring Trends in Burn Severity [MTBS] (2025)[4]	4600	1000*
MMC	Proportion mesic mixed-conifer forest	LANDFIRE (2018)	2100*	900*
QMD	Quadratic mean diameter in cm (all trees)	Sesnie et al. (2006)[1]	4300	1000
RdNBR	Mean value of Relative delta Normalized Burn Ratio	Monitoring Trends in Burn Severity [MTBS], 2025	5000	400
Salvage	Proportion of area salvage logged	USFS GIS databases (U.S. Forest Service, 2018a,b)[5,6]	4000	700
Slope	Mean slope in degrees	U.S. Geological Survey (2014)[7]	500*	500*

[1] Data directly acquired from S. E. Sesnie and his research team.
[2] National Land Cover Database, Homer et al., 2015
[3] LANDFIRE Existing Vegetation Type Layer 2014.
[4] Monitoring Trends in Burn Severity Data Access Fire Level Geospatial Data 2014*b*.
[5] Apache-Sitgreaves National Forest GIS data 2018. (U.S. Forest Service, 2018a)
[6] Tonto National Forest GIS data 2018. (U.S. Forest Service, 2018b)
[7] National Elevation Dataset, U.S. Geological Survey, 2014

Table 2
Predictor variables and their optimized scales for multi-scale analysis in LiDAR-focused models. The optimal scale represents the radius at which each variable exhibited the strongest relationship with the presence of Mexican spotted owls, as determined by out-of-bag error rates. Mean values are based on a 10-m pixel size. The year column indicates when data were collected. Variables included in the final model are marked in the optimal scale column with an asterisk (*).

Predictor	Units and definition	Source (year)	Optimal scale (m)	
			Home range (2nd order)	Microhabitat (3rd order)
BA (≥30-cm)	Mean basal area in m^2/ha of trees ≥30-cm DBH	LiDAR (2013/14)	200	200
BA (≥46-cm)	Mean basal area in m^2/ha of trees ≥46-cm DBH	LiDAR (2013/14)	100	400
BA (≥60-cm)	Mean basal area in m^2/ha of trees ≥60-cm DBH	LiDAR (2013/14)	5000	500
CC (≥16-m)	Percent canopy cover at ≥16-m height	LiDAR (2013/14)	4900	300
CC (2–16-m)	Percent canopy cover from 2 to 16-m height	LiDAR (2013/14)	3900	400
DBH (≥30-cm)	Number of trees ≥30-cm DBH	LiDAR (2013/14)	4800	200*
DBH (>46-cm)	Number of trees ≥46-cm DBH	LiDAR (2013/14)	2200	300
DBH (>60-cm)	Number of trees ≥60-cm DBH	LiDAR (2013/14)	100*	300
DMC	Proportion dry mixed-conifer forest cover	LANDFIRE (2018)[1]	2000*	1000*
HSF	Percent area burned at high severity	Monitoring Trends in Burn Severity [MTBS] (2025)[2]	4300	1000
MMC	Proportion mesic mixed-conifer forest	LANDFIRE, 2018	3100*	800*
RdNBR	Mean value of Relative delta Normalized Burn Ratio	LANDFIRE (2018)	3700	200
Salvage	Proportion of area salvage logged	USFS GIS database (U.S. Forest Service, 2018a,b)[3,4]	4000	700
Slope	Mean slope in degrees	LiDAR (2013/14)	4200*	500
Snags (≥20-m)	Number of dead trees ≥20-m in height	LiDAR (2013/14)	3700	800
Live trees (≥20-m)	Number of live trees >20-m in height	LiDAR (2013/14)	100	200

[1] LANDFIRE Existing Vegetation Type Layer 2018.
[2] Monitoring Trends in Burn Severity Data Access Fire Level Geospatial Data 2014*b*.
[3] Apache-Sitgreaves National Forest GIS data 2018. (U.S. Forest Service, 2018a)
[4] Tonto National Forest GIS data 2018. (U.S. Forest Service, 2018b)

of 2100 m and 3100 m, respectively.

In LANDSAT-based microhabitat selection models, BA, CC, and QMD were most predictive at 100 m, 500 m, and 1000 m, respectively. RdNBR was optimized at 400 m, while the DMC and MMC were most influential at scales of 900 m. Fire and logging-related variables, including HSF and salvage logging, were optimized at 700 m and 1000 m, respectively.

For LiDAR-based home range selection models, the most predictive spatial scales for LiDAR-derived covariates ranged widely. Key predictors such as BA of large trees (≥60 cm DBH) and CC >16 m were most influential at broad scales (5000 m and 4900 m, respectively). In contrast, the number of live trees ≥20 m tall and BA of trees ≥30 cm DBH were most predictive at finer scales of 100 m and 200 m, respectively. Slope and RdNBR were optimized at intermediate scales of 4200 m and 3700 m.

For LiDAR-based microhabitat selection models, predictors were generally optimized at fine scales. For instance, the number of live trees ≥20 m tall and BA of large trees (≥30 cm DBH) were strongly associated with owl presence at 200 m. CC variables, both ≥16 m and 2–16 m, were optimized at 300 m and 400 m, respectively. Also, RdNBR was most influential at a fine scale of 200 m. Meanwhile, DMC, MMC, HSF, and the number of snags were optimized at larger scales from 800 to 1000 m.

3.2. Multicollinearity analysis

For LANDSAT-based models, many variables were highly correlated (Figs. S1, S3). For example, CC and BA were highly correlated at home range level ($|r| \geq 0.82$), and CC was retained. Fire-related variables, including RdNBR and HSF, were correlated at both levels ($|r| = 0.93$ and 0.80), and RdNBR was retained.

For LiDAR-based models, several variables showed high correlation (i.e., $r > |0.7|$) at home range and microhabitat levels (Figs. S2, S4). For instance, BA metrics for trees ≥30 cm, ≥46 cm, and ≥ 60 cm DBH were highly correlated ($|r| \geq 0.83$), with BA ≥30 cm retained due to its stronger relationship with owl presence. Similarly, CC metrics at different height strata (CC ≥16 m and CC 2–16 m) were strongly correlated at home range level ($|r| = 0.81$), and CC ≥16 m was retained. Tree density metrics for DBH ≥30 cm, ≥46 cm, and ≥ 60 cm also exhibited high correlations ($|r| \geq 0.78$), with DBH ≥30 cm retained for its higher predictive power. Among fire-related variables, HSF and RdNBR were highly and moderately correlated at home range and microhabitat levels, respectively ($|r| = 0.95$ and 0.72), and RdNBR was retained.

3.3. Variable importance

Variable importance rankings revealed that certain predictors, such as MMC and DMC forests, consistently ranked highly across all final models (Fig. 3). Slope also emerged as a key variable in three of the four models. These findings underscore the critical role of these variables in influencing habitat selection of the Mexican spotted owl, and suggest a general relationship of higher suitability for Mexican spotted owls in areas of high cover of these forest types on steep slopes.

3.4. Habitat selection

Habitat selection patterns for Mexican spotted owls, as illustrated in the partial dependence plots (Figs. S5–S8), reveal nuanced relationships between key predictors and habitat suitability across models. CC shows

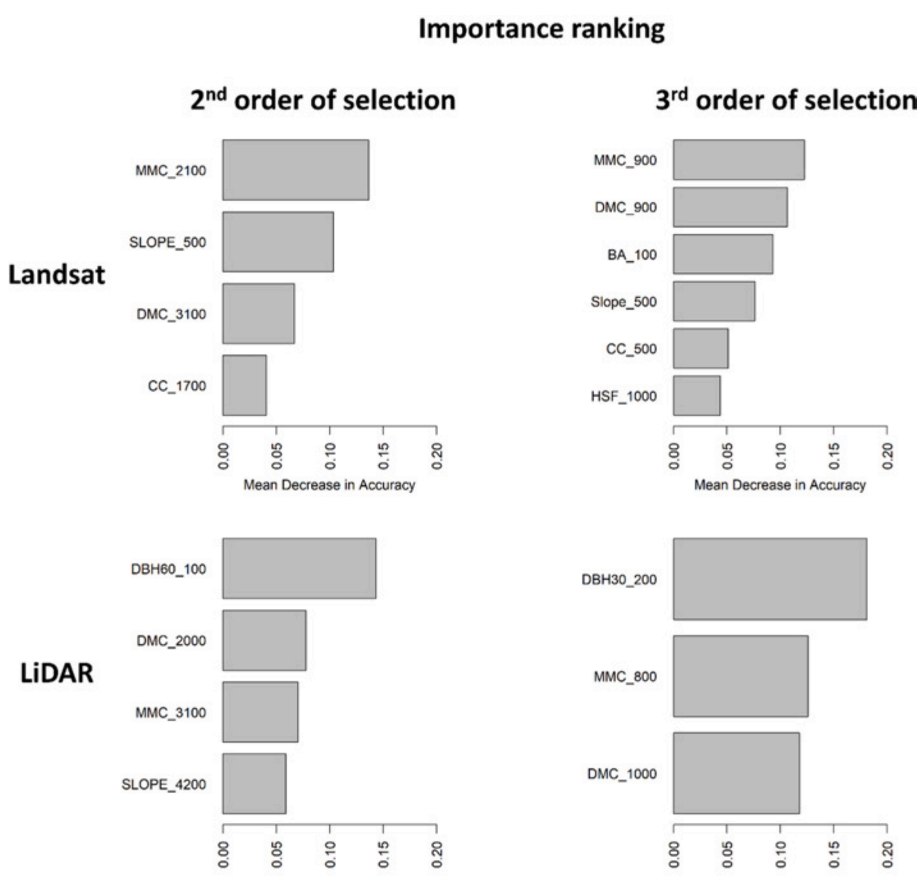

Fig. 3. Importance rankings of predictor variables for home range level (2nd order) and microhabitat level (3rd order) habitat selection models of Mexican spotted owls across all orders of selection (columns) and datasets (rows). Rankings are based on the mean percent decrease in classification accuracy, calculated by permuting each variable individually to evaluate its contribution to model performance.

a non-linear relationship for the home range level LANDSAT model, with suitability increasing at intermediate canopy values before declining. DMC and MMC show positive, slightly non-linear association with habitat suitability. Slope demonstrates a clear positive relationship, with suitability increasing at steeper slopes, and then declines past an optimal peak. For microhabitat selection, high level of BA shows a positive relationship with suitability, while CC shows a non-linear relationship, with intermediate values being most favorable. DMC and MMC forests both show positive, slightly non-linear relationships with suitability. HSF also shows a non-linear trend, with suitability peaking at intermediate proportions of HSF and generally low probability as the proportion of HSF exceeds 0.4. Slope displays a non-linear pattern, with moderate slopes associated with the highest suitability.

For the LiDAR-based home range selection model, slope shows a clear positive relationship with suitability at steeper slopes. MMC exhibits a non-linear trend, with higher proportions moderately contributing to habitat suitability. DMC displays a complex, non-linear relationship, with suitability peaking at intermediate and higher values. Finally, the density of trees ≥60 cm DBH shows a strong relationship with habitat suitability. For microhabitat selection, MMC is positively associated with habitat suitability. DMC again exhibits a non-linear relationship, peaking at intermediate values before declining slightly at higher proportions. The density of trees ≥30 cm DBH also shows a non-linear effect, with suitability increasing at intermediate densities and plateauing at higher values.

3.5. Model performance

Overall, both LANDSAT-based and LiDAR based models performed comparably well with neither dataset exhibiting a significant advantage over the other (Table 3). LANDSAT-based models consistently demonstrated slightly higher or equal performance metrics across both orders of selection, but the differences in performance were relatively small.

3.6. Spatial predictions and disagreement

Spatial predictions of habitat suitability differed between LANDSAT- and LiDAR-based models. For home range level models (Figs. 4a, c), LANDSAT predictions emphasized broader regions of high suitability, whereas LiDAR predictions highlighted more localized high-suitability areas. For microhabitat level models (Figs. 4b, d), LiDAR continued to provide finer-resolution hotspots, capturing small-scale variations in habitat suitability more effectively than LANDSAT.

The spatial disagreement analysis revealed general agreement between the two datasets, with some regions showing notable disagreement (Figs. 5, 6). For home range level models, areas of high disagreement were concentrated in the southwestern portion of the study area. For microhabitat level models, most PACs exhibited minimal disagreement, though some PACs showed high disagreement in small, highly localized areas. We suspect that these discrepancies likely stem from differences in the temporal coverage of the forest GIS layers used for the two datasets. For instance, LANDSAT-derived basal area data were created in 2006, while LiDAR products were based on data collected in 2013–2014. These temporal differences may account for variations in forest structure and composition, and thus habitat prediction, captured by each dataset.

3.7. Key findings summary

Overall, our results show that Mexican spotted owl habitat selection patterns were consistently associated with forest composition, structure, and topography across both remote sensing approaches, although the optimized spatial scales and variable importance differed between LiDAR- and LANDSAT-based models (Fig. 3). Despite these differences, both LiDAR- and LANDSAT-derived models exhibited similar predictive accuracy. Spatial predictions revealed that LANDSAT-based models emphasized broader regions of habitat suitability, while LiDAR-based models highlighted more localized habitat hotspots, particularly at the microhabitat scale (Fig. 4).

4. Discussion

4.1. Integrating scale optimization to leverage remote sensing products strengths in habitat suitability modeling

It is well established that spatial scale influences the accuracy and ecological relevance of habitat suitability models and our understanding of how species interact with habitat features across multiple spatial levels and scales (McGarigal et al., 2016). However, little research has examined how scale affects the performance of different remote sensing data products, such as lower-resolution LANDSAT versus higher-resolution LiDAR, in habitat suitability modeling. Our multi-scale, multi-level study addresses this critical knowledge gap and underscores the importance of incorporating spatial scale considerations when using remotely sensed data for habitat suitability modeling.

Many studies have highlighted the advantages of high-resolution LiDAR data for environmental monitoring, often demonstrating that LiDAR outperforms or complements coarser-resolution products like LANDSAT. For example, LiDAR enhances biomass monitoring by calibrating LANDSAT time-series data, improving estimates of forest carbon stocks (Pflugmacher et al., 2014). It also enables precise subpixel inundation mapping, improving LANDSAT's ability to track wetland changes over time for large-scale, long-term monitoring (Huang et al., 2014). Additionally, LiDAR provides detailed forest structure data over large areas with accuracy comparable to traditional stand exams but with broader spatial coverage (Hummel et al., 2011). Its superior accuracy in estimating tree cover and height further makes LiDAR essential for precise forest extent mapping and monitoring (Tang et al., 2019).

Given these strengths, it is often assumed that LiDAR will always outperform other data products of lower resolution for species habitat suitability modeling. However, this assumption is underexplored, particularly in studies comparing LANDSAT and LiDAR, which are often constrained to single-scale frameworks. Ackers et al. (2015), for example, compared habitat maps for northern spotted owls using MAXENT with LANDSAT and LiDAR data in a single-scale approach where all variables were fixed at a 30-m resolution. As expected, their findings supported the conventional wisdom, showing that LiDAR-based maps outperformed LANDSAT-based maps in terms of gain, AUC, and spatial precision. However, our study reveals that the degree of improvement with LiDAR depends on the scales at which data are

Table 3
Cross-validated performance metrics for home range selection (2nd order) and microhabitat selection (3rd order) models of Mexican spotted owls using LANDSAT- and LiDAR-derived data. Threshold refers to the predicted probability cutoff for classifying presence. Metrics include percent correctly classified (PCC), sensitivity (true positive rate), specificity (true negative rate), Kappa (agreement beyond chance), area under the curve (AUC), and out-of-bag error rate (OOB).

Model	Data	Threshold	PCC	Sensitivity	Specificity	Kappa	AUC	OOB
Home range selection (2nd Order)	Landsat	0.570	0.968	0.908	0.984	0.903	0.976	0.037
	LiDAR	0.410	0.958	0.908	0.971	0.876	0.975	0.050
Microhabitat selection (3rd Order)	Landsat	0.619	0.948	0.920	0.977	0.897	0.971	0.057
	LiDAR	0.695	0.931	0.897	0.966	0.862	0.972	0.092

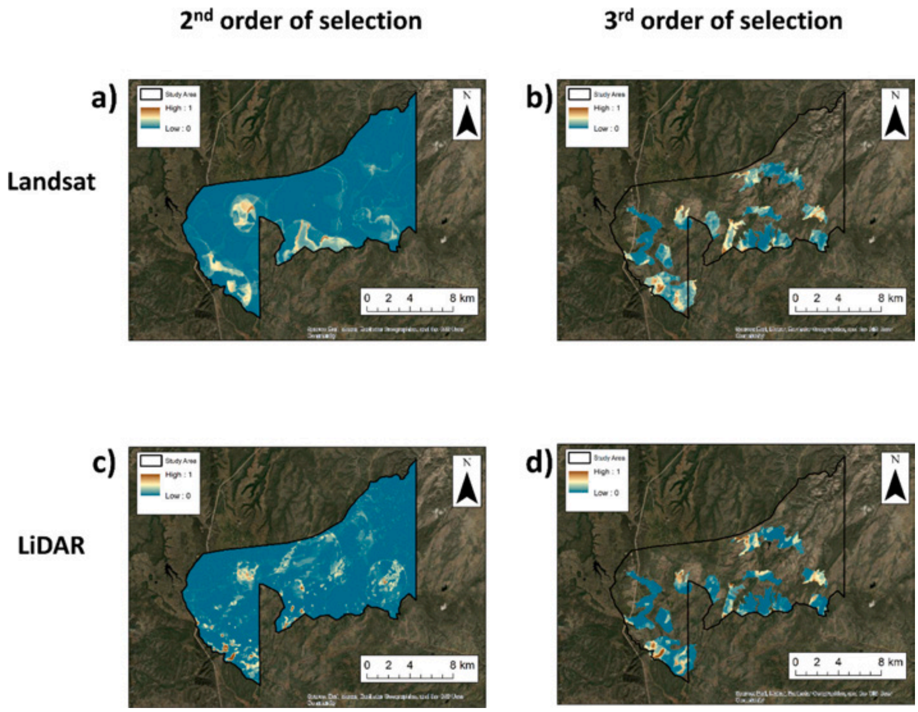

Fig. 4. Predicted habitat suitability for Mexican spotted owls within the study area at home range level (2nd order) and microhabitat level (3rd order) using LANDSAT- and LiDAR-based models. Panels (a) and (b) show predictions for home range level and microhabitat level LANDSAT-based models, respectively, while panels (c) and (d) represent predictions for home range level and microhabitat level LiDAR-based models.

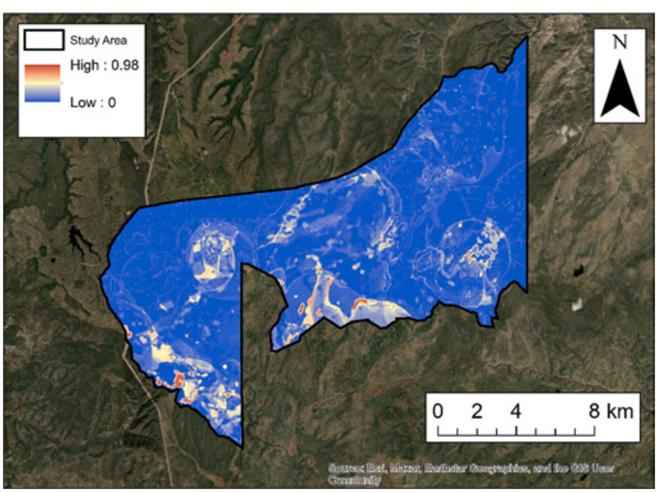

Fig. 5. Spatial disagreement between LANDSAT- and LiDAR-based habitat selection models for Mexican spotted owls within the study area at the home range level (2nd order of selection). The map depicts the absolute difference in predicted habitat suitability values between the two models. Cooler colors (values closer to 0) indicate low disagreement, while warmer colors (values closer to 1) highlight areas of high disagreement.

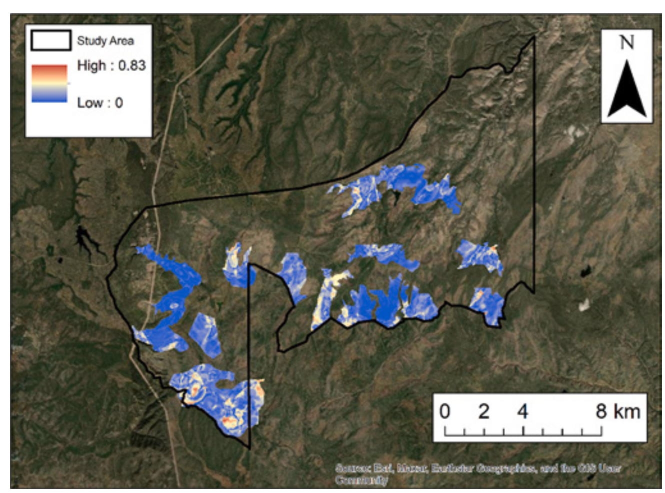

Fig. 6. Spatial disagreement between LANDSAT- and LiDAR-based habitat selection models for Mexican spotted owls at the microhabitat level (3rd order of selection). Habitat was modeled only within the boundaries of owl Protected Activity Centers here. The map depicts the absolute difference in predicted habitat suitability values between the two models. Cooler colors (values closer to 0) indicate low disagreement, while warmer colors (values closer to 1) highlight areas of high disagreement.

analyzed. By incorporating a multi-scale framework, optimizing predictors across a range of ecologically meaningful scales, and examining multi-level habitat selection (i.e., home range level and microhabitat level), we captured nuanced patterns of habitat use that would have been overlooked in a fixed-scale approach.

Our findings demonstrate that when models are scale-optimized, both LANDSAT and LiDAR perform equally well in predicting suitability for Mexican spotted owls, despite their differences in resolution and data characteristics. In fact, the spatial predictions produced by the two datasets generally align except in areas with very complex topography and forest composition (Figs. 5, 6). This highlights the importance of scale optimization in leveraging the unique strengths of diverse remote sensing products for habitat suitability modeling. By addressing the interplay of scale and data resolution, our study provides a more nuanced understanding of the applications of these products in species conservation and further emphasizes the critical role of scale in determining the efficacy of remote sensing in habitat suitability modeling.

4.2. Monitoring habitat in post-fire landscapes

Wildfires are increasingly severe and widespread, with fire regimes deviating significantly from historical norms in many regions (Hantson et al., 2024). Assessing the habitat changes caused by these fires is essential for effective species management and conservation. This study provides valuable insights into habitat management in post-fire landscapes, particularly for the Mexican spotted owl. Mexican spotted owl is often thought to be a mature forest habitat specialist, which is highly vulnerable to large, high-severity fires (e.g., Wan et al., 2019b, 2020). By understanding how habitat preferences vary across spatial scales and data sources, land managers can develop conservation strategies tailored to the needs of this species.

The relationship between spotted owls and wildfire is complex (Ganey et al., 2017). Evidence suggests that low- and moderate-severity fires generally have little impact on spotted owls (Bond, 2016; Ganey et al., 2017). Our results indicate that high-severity fires are not inherently incompatible with Mexican spotted owls, but their effects depend on the scale of analysis and spatial location. Fire-related covariates, such as high-severity fire (HSF) and RdNBR, were largely absent from the final models, except microhabitat level LANDSAT model (Fig. 3). This may indicate that other variables, such as the availability of mixed-conifer forests, are more limiting and thus drive habitat selection, or that the remaining landscape features may be more important to owls than the features that was lost.

The broad scales optimized in the home range level models suggest that large, contiguous patches of high-severity fire are most likely to impact Mexican spotted owls at the population level. In addition, we show that key structural elements such as high basal area, large trees, and canopy cover should be preserved at fine scales around nest and roost sites to maintain suitable habitat while still managing for resilience to fire.

In the post-fire landscape, Mexican spotted owls generally selected habitat elements similar to those used for nesting and roosting in unburned areas, including large trees, high canopy cover, and mixed-conifer forests (Ganey et al., 2013; Grubb et al., 1997; May et al., 2004; Seamans and Gutiérrez, 1995; Timm et al., 2016; Wan et al., 2017, 2019a). However, these habitat features may be less abundant after fires. Owls may persist in or colonize small patches of mature mixed-conifer forest or networks of smaller patches in the absence of larger contiguous areas. Managers should prioritize the protection of these smaller habitat patches following fire events.

Despite these findings, it remains uncertain whether post-fire landscapes provide sufficient habitat quantity and quality to support viable owl populations. Long-term studies of owl demography and habitat relationships in post-fire environments are essential to address this question (Ganey et al., 2017; Wan et al., 2018). The scale-optimized models developed in this study provide a robust framework for prioritizing areas for restoration and protection, particularly regions with high proportions of mesic mixed-conifer forests or steep slopes.

Furthermore, the long-term sustainability of LiDAR acquisition at consistent intervals remains a significant challenge due to the high costs and logistical constraints of repeated data collection, particularly in achieving wall-to-wall coverage across landscapes. Temporal and spatial mismatches between LiDAR data and wildlife detections underscore potential limitations for long-term monitoring of Mexican spotted owls and other wildlife species. Until LiDAR becomes widely available with sufficient temporal coverage, the broad temporal coverage of LANDSAT data remains valuable. Finally, as demonstrated by this study, integrating LANDSAT and LiDAR data provides a scalable and cost-effective approach for monitoring habitat recovery over large areas while maintaining predictive accuracy.

4.3. Limitations and future directions

Inherent differences between LANDSAT and LiDAR determine the available covariates for modeling. While we used the same covariates where possible, full consistency was not achievable. Future research could explore data fusion techniques to better integrate spectral and structural information. Second, we used a single modeling approach (i.e., RF) and focused solely on habitat suitability because RF can handle complex ecological data, capture non-linear relationships, and minimize overfitting. Many studies comparing regression-based and machine learning-based habitat models have demonstrated that RF often achieves superior predictive accuracy (Cushman et al., 2017; Cushman and Wasserman, 2018; Hysen et al., 2022; Kumar et al., 2021). Additionally, RF has been shown to outperform ensemble models when the ratio of background points to presence points falls within an optimal range (e.g., X1 to X10 times the presence points; Hysen et al., 2022). Given these considerations, RF was the most suitable choice for our study. Future studies could compare LiDAR and LANDSAT products using alternative statistical methods, such as regression-based models, ensemble modeling, and other frameworks like occupancy and connectivity models. Finally, although we used the closest available datasets to minimize biases from temporal mismatches between LiDAR and LANDSAT, some discrepancies may remain. However, we believe these biases are minimal, as no major landscape changes occurred during that period. As LiDAR and LANDSAT products continue to improve in spatial and temporal coverage, such discrepancies should diminish. We encourage future studies to use temporally matched datasets whenever possible.

CRediT authorship contribution statement

Ho Yi Wan: Writing – review & editing, Writing – original draft, Visualization, Validation, Supervision, Software, Project administration, Methodology, Investigation, Formal analysis, Data curation, Conceptualization. **Michael A. Lommler:** Writing – review & editing, Writing – original draft, Investigation, Formal analysis, Data curation, Conceptualization. **Samuel A. Cushman:** Writing – review & editing, Methodology, Conceptualization. **Jamie S. Sanderlin:** Writing – review & editing. **Joseph L. Ganey:** Writing – review & editing, Funding acquisition, Data curation, Conceptualization. **Andrew J. Sánchez Meador:** Writing – review & editing, Methodology, Data curation, Conceptualization. **Paul Beier:** Writing – review & editing, Conceptualization.

Declaration of competing interest

The authors declare that they have no known competing financial interests or personal relationships that could have appeared to influence the work reported in this paper.

Appendix A. Supplementary data

Supplementary data to this article can be found online at https://doi.org/10.1016/j.ecoinf.2025.103168.

Data availability

The data and code used in this research are available on the Zenodo repository at https://zenodo.org/records/15049098

References

Ackers, S.H., Davis, R.J., Olsen, K.A., Dugger, K.M., 2015. The evolution of mapping habitat for northern spotted owls (*Strix occidentalis caurina*): a comparison of photo-interpreted, Landsat-based, and lidar-based habitat maps. Remote Sens. Environ. 156, 361–373. https://doi.org/10.1016/j.rse.2014.09.025.

Balch, J.K., Bradley, B.A., Abatzoglou, J.T., Nagy, R.C., Fusco, E.J., Mahood, A.L., 2017. Human-started wildfires expand the fire niche across the United States. Proc. Natl. Acad. Sci. 114 (11), 2946–2951. https://doi.org/10.1073/pnas.1617394114.

Balch, J.K., Iglesias, V., Mahood, A.L., Cook, M.C., Amaral, C., DeCastro, A., Leyk, S., McIntosh, T.L., Nagy, R.C., Denis, L.S., et al., 2024. The fastest-growing and most

destructive fires in the US (2001 to 2020). Science 386 (425–431). https://doi.org/10.1126/science.adk5737.
Blackburn, R.C., Buscaglia, R., Sanchez Meador, A.J., 2021. Mixtures of airborne LiDAR-based approaches improve predictions of forest structure. Can. J. For. Res. 51 (8), 1106–1116. https://doi.org/10.1139/cjfr-2020-0506.
Bond, M.L., 2016. The heat is on: spotted owls and wildfire. In: Reference Module in Earth Systems and Environmental Sciences. https://doi.org/10.1016/B978-0-12-409548-9.10014-4.
Breiman, T., Cutler, A., 2011. Package "randomForest". https://CRAN.R-project.org/package=randomForest.
Collins, L., Bradstock, R.A., Clarke, H., Clarke, M.F., Nolan, R.H., Penman, T.D., 2021. The 2019/2020 mega-fires exposed Australian ecosystems to an unprecedented extent of high-severity fire. Environ. Res. Lett. 16 (4), 044029. https://doi.org/10.1088/1748-9326/abeb9e.
Cushman, S.A., Wasserman, T.N., 2018. Landscape applications of machine learning: comparing random forests and logistic regression in multi-scale optimized predictive modeling of American marten occurrence in northern Idaho, USA. In: Machine Learning for Ecology and Sustainable Natural Resource Management, pp. 185–203. https://doi.org/10.1007/978-3-319-96978-7_9.
Cushman, S.A., Macdonald, E.A., Landguth, E.L., Malhi, Y., Macdonald, D.W., 2017. Multiple-scale prediction of forest loss risk across Borneo. Landsc. Ecol. 32, 1581–1598. https://doi.org/10.1007/s10980-017-0520-0.
Cushman, S.A., Kaszta, Z.M., Burns, P., Hakkenberg, C.R., Jantz, P., Macdonald, D.W., Brodie, J.F., Deith, M.C.M., Goetz, S., 2024. Simulating multi-scale optimization and variable selection in species distribution modeling. Eco. Inform. 83, 102832. https://doi.org/10.1016/j.ecoinf.2024.102832.
Dickson, B.G., Sisk, T.D., Sesnie, S.E., Reynolds, R.T., Rosenstock, S.S., Vojta, C.D., Ingraldi, M.F., Rundall, J.M., 2014. Integrating single-species management and landscape conservation using regional habitat occurrence models: the northern goshawk in the southwest, USA. Landsc. Ecol. 29, 803–815. https://doi.org/10.1007/s10980-014-0013-3.
Dillon, G.K., Holden, Z.A., Morgan, P., Crimmins, M.A., Heyerdahl, E.K., Luce, C.H., 2011. Both topography and climate affected forest and woodland burn severity in two regions of the western US, 1984 to 2006. Ecosphere 2 (12), 130. https://doi.org/10.1890/ES11-00271.1.
Driscoll, D.A., Armenteras, D., Bennett, A.F., Brotons, L., Clarke, M.F., et al., 2021. How fire interacts with habitat loss and fragmentation. Biol. Rev. 96, 976–998. https://doi.org/10.1111/brv.12687.
Environmental Systems Research Institute [ESRI], 2017. ArcGIS for Desktop 10.6.
Forsman, E.D., 1983. Methods and Materials for Locating and Studying Spotted Owls. General Technical Report PNW-162,. USDA Forest Service Pacific Northwest Forest and Range Experiment Station.
Galbraith, S.M., Valente, J.J., Dunn, C.J., Rivers, J.W., 2024. Both Landsat-and LiDAR-derived measures predict forest bee response to large-scale wildfire. Remote Sens. Ecol. Conserv. 10 (1), 24–38. https://doi.org/10.1016/j.rse.2009.03.004.
Ganey, J.L., Apprill, D.L., Rawlinson, T.A., Kyle, S.C., Jonnes, R.S., Ward, J.P., 2013. Nesting habitat of Mexican spotted owls in the Sacramento Mountains, New Mexico. J. Wildl. Manag. 77 (7), 1426–1435. https://doi.org/10.1002/jwmg.599.
Ganey, J.L., Wan, H.Y., Cushman, S.A., Vojta, C.D., 2017. Conflicting perspectives on spotted owls, wildfire, and forest restoration. Fire Ecol. 13 (3), 146–165. https://doi.org/10.4996/fireecology.130318020.
Garcia-Feced, C., Tempel, D.J., Kelly, M., 2011. LiDAR as a tool to characterize wildlife habitat: California spotted owl nesting habitat as an example. J. For. 2011, 436–443. https://doi.org/10.1093/jof/109.8.436. December.
Grubb, T.G., Ganey, J.L., Masek, S.R., 1997. Canopy closure around nest sites of Mexican spotted owls in northcentral Arizona. J. Wildl. Manag. 61 (2), 336–342. https://doi.org/10.2307/3802589.
Gutiérrez, R.J., Franklin, A.B., Lahaye, W.S., 1995. Spotted owl (*Strix occidentalis*). In: Poole, A., Gill, F. (Eds.), The Birds of North America No. 179: Life Histories for the 21st Century. The Philadelphia Academy of Sciences; The American Ornithologists' Union, Washington, D.C.
Hagmann, R.K., Hessburg, P.F., Prichard, S.J., Povak, N.A., Brown, P.M., Fulé, P.Z., Keane, R.E., Knapp, E.E., Lydersen, J.M., Metlen, K.L., Reilly, M.J., 2021. Evidence for widespread changes in the structure, composition, and fire regimes of western North American forests. Ecol. Appl. 31 (8), e02431. https://doi.org/10.1002/eap.2431.
Hantson, S., Hamilton, D.S., Burton, C., 2024. Changing fire regimes: ecosystem impacts in a shifting climate. One Earth 7 (6), 942–945. https://doi.org/10.1016/j.oneear.2024.05.021.
Heidemann, H., 2012. LiDAR base specification. In: Collection and Delineation of Spatial Data. USGS. https://pubs.usgs.gov/tm/11b4/pdf/tm11-B4.pdf.
Higuera, P.E., 2015. Taking time to consider the causes and consequences of large wildfire. PNAS 112 (43), 13137–13138. https://doi.org/10.1073/pnas.1518170112.
Holden, Z.A., Morgan, P., Rollins, M.G., Evans, J.S., 2009. A predictive model of burn severity based on 20-year satellite-inferred burn severity data in a large southwestern US wilderness area. For. Ecol. Manag. 258, 2399–2406. https://doi.org/10.1016/j.foreco.2009.08.017.
Homer, C.G., Dewitz, J.A., Yang, L., Jin, S., Danielson, P., Xian, G., Coulston, J., Herold, N.D., Wickham, J.D., Megown, K., 2015. Completion of the 2011 National Land Cover Database for the conterminous United States—representing a decade of land cover change information. Photogramm. Eng. Remote. Sens. 81 (5), 345–354. https://doi.org/10.1016/S0099-1112(15)30100-2.
Horn, B.K.P., 1981. Hill shading and the reflectance map. Proc. IEEE 69 (1), 14–47. https://doi.org/10.1109/PROC.1981.11918.
Huang, C., Peng, Y., Lang, M., Yeo, I.-Y., McCarty, G., 2014. Wetland inundation mapping and change monitoring using Landsat and airborne LiDAR data. Remote Sens. Environ. 141, 231–242. https://doi.org/10.1016/j.rse.2013.10.020.
Hummel, S., Hudak, A.T., Uebler, E.H., Falkowski, M.J., Megown, K.A., 2011. A comparison of accuracy and cost of LiDAR versus stand exam data for landscape management on the Malheur national forest. J. For. 109 (5), 267–273. https://doi.org/10.1093/jof/109.5.267.
Hysen, L., Nayeri, D., Cushman, S., Wan, H.Y., 2022. Background sampling for multi-scale ensemble habitat selection modeling: does the number of points matter? Eco. Inform. 72, 101914. https://doi.org/10.1016/j.ecoinf.2022.101914.
Hysen, L.B., Cushman, S.A., Fogarty, F.A., Kelly, E.C., Nayeri, D., Wan, H.Y., 2023. Northern spotted owl nesting habitat under high potential wildfire threats along the California coastal redwood forest. Sci. Total Environ. 890, 163414. https://doi.org/10.1016/j.scitotenv.2023.163414.
Jenness, J., 2013. DEM surface tools. In: Jenness Enterprises. http://www.jennessent.com/arcgis/surface_area.htm.
Johnson, D.H., 1980. The comparison of usage and availability measurements for evaluating resource preference. Ecology 61, 65–71. https://doi.org/10.2307/1937156.
Jones, M.W., Abatzoglou, J.T., Veraverbeke, S., Andela, N., Lasslop, G., Forkel, M., Smith, A.J.P., Burton, C., Betts, R.A., van der Werf, G.R., Sitch, S., Canadell, J.G., Santín, C., Kolden, C., Doerr, S.H., Le Quéré, C., 2022. Global and regional trends and drivers of fire under climate change. Rev. Geophys. 60, e2020RG000726. https://doi.org/10.1029/2020RG000726.
Khosravi, R., Pourghasemi, H.R., Adavoudi, R., Julaie, L., Wan, H.Y., 2022. A spatially explicit analytical framework to assess wildfire risks on brown bear habitat and corridors in conservation areas. Fire Ecol. 18 (1), 1–14. https://doi.org/10.1186/s42408-021-00125-0.
Kramer, A., Jones, G.M., Whitmore, S.A., Keane, J.J., Atuo, F.A., Dotters, B.P., Peery, M. Z., 2021. California spotted owl habitat selection in a fire-managed landscape suggests conservation benefit of restoring historical fire regimes. For. Ecol. Manag. 479, 118576. https://doi.org/10.1016/j.foreco.2020.118576.
Kumar, S.U., Maini, P.K., Chiaverini, L., Hearn, A.J., Macdonald, D.W., Kaszta, Ż., Cushman, S.A., 2021. Smoothing and the environmental manifold. Eco. Inform. 66, 101472. https://doi.org/10.1016/j.ecoinf.2021.101472.
LANDFIRE, 2018. LANDFIRE Existing Vegetation Type Layer. U.S. Department of Interior, Geological Survey. https://www.landfire.gov/viewer/.
Li, W., Guo, Q., Jakubowski, M.K., Kelly, M., 2012. A new method for segmenting individual trees from the lidar point cloud. Photogramm. Eng. Remote. Sens. 78 (1), 75–84. https://doi.org/10.14358/PERS.78.1.75.
May, C.A., Petersburg, M.L., Gutiérrez, R.J., 2004. Mexican spotted owl nest- and roost-site habitat in northern Arizona. J. Wildl. Manag. 68, 1054–1064. https://doi.org/10.2193/0022-541X(2004)068[1054:MSONAR]2.0.CO;2.
McGarigal, K., Wan, H.Y., Zeller, K.A., Timm, B.C., Cushman, S.A., 2016. Multi-scale habitat modeling: a review and outlook. Landsc. Ecol. 31 (6), 1161–1175. https://doi.org/10.1007/s10980-016-0374-x.
Miller, J.D., Thode, A.E., 2007. Quantifying burn severity in a heterogeneous landscape with a relative version of the delta normalized burn ratio (dNBR). Remote Sens. Environ. 109 (1), 66–80. https://doi.org/10.1016/j.rse.2006.12.006.
Monitoring Trends in Burn Severity [MTBS], 2025. Monitoring Trends in Burn Severity (MTBS) Project Data Access: Fire Level Geospatial Data. U.S. Forest Service and U.S. Geological Survey. https://www.mtbs.gov/direct-download.
Moran, C.J., Kane, V.R., Seielstad, C.A., 2020. Mapping forest canopy fuels in the Western United States with LiDAR–Landsat covariance. Remote Sens. 12 (6), 1000. https://doi.org/10.3390/rs12061000.
National Land Cover Dataset [NLCD], 2011. NLCD 2011 USFS Tree Canopy Cover CONUS. U.S. Geological Survey. https://www.mrlc.gov/data/nlcd-2011-usfs-tree-canopy-cover-conus-0.
Nayeri, D., Cushman, S., Ganey, J., Hysen, L., Gunther, M.S., Willey, D., Wan, H.Y., 2024. Multiscale habitat suitability modeling for a threatened raptor offers insight into ecological model transferability. Ecol. Model. 496, 110845. https://doi.org/10.1016/j.ecolmodel.2024.110845.
North, M.P., Kane, J.T., Kane, V.R., Asner, G.P., Berigan, W., Churchill, D.J., Conway, S. T., Gutierrez, R.J., Jeronimo, S., Keane, J., Koltunove, A., Mark, T., Moskal, M., Munton, T., Peery, Z., Ramirez, C., Sollmann, R., White, A.M., Whitmore, S., 2017. Cover of tall trees best predicts California spotted owl habitat. For. Ecol. Manag. 405, 166–178. https://doi.org/10.1016/j.foreco.2017.09.019.
Pflugmacher, D., Cohen, W.B., Kennedy, R.E., Yang, Z., 2014. Using Landsat-derived disturbance and recovery history and LiDAR to map forest biomass dynamics. Remote Sens. Environ. 151, 124–137. https://doi.org/10.1016/j.rse.2013.05.033.
Roberts, S.L., van Wagtendonk, J.W., Miles, A.K., Kelt, D.A., 2011. Effects of fire on spotted owl site occupancy in a late-successional forest. Biol. Conserv. 144, 610–619. https://doi.org/10.1016/j.biocon.2010.11.002.
Roussel, J.R., Auty, D., 2023. Airborne LiDAR data manipulation and visualization for forestry applications. In: R Package Version 3.1.0. https://cran.r-project.org/package=lidR.
Roussel, J.R., Auty, D., Coops, N.C., Tompalski, P., Goodbody, T.R.H., Sánchez Meador, A., Bourdon, J.F., De Boissieu, F., Achim, A., 2020. lidR: an R package for analysis of airborne laser scanning (ALS) data. Remote Sens. Environ. 251, 112061. https://doi.org/10.1016/j.rse.2020.112061.
Seamans, M.E., Gutiérrez, R.J., 1995. Breeding habitat ecology of the Mexican spotted owl in the Tularosa Mountains, New Mexico. Condor 97, 944–952. https://doi.org/10.2307/1369533.
Seavy, N.E., Viers, J.H., Wood, J.K., 2009. Riparian bird response to vegetation structure: a multiscale analysis using LiDAR measurements of canopy height. Ecol. Appl. 19 (7), 1848–1857. https://doi.org/10.1890/08-1124.1.

Singleton, M.P., Thode, A.E., Sánchez Meador, A.J., Iniguez, J.M., 2019. Increasing trends in high-severity fire in the southwestern USA from 1984 to 2015. For. Ecol. Manag. 433, 709–719. https://doi.org/10.1016/j.foreco.2018.11.039.

Stephens, S.L., Burrows, N., Buyantuyev, A., Gray, R.W., Keane, R.E., Kubian, R., Liu, S., Seijo, F., Shu, L., Tolhurst, K.G., van Wagtendonk, J.W., 2014. Temperate and boreal forest mega-fires: characteristics and challenges. Front. Ecol. Environ. 12, 115–122. https://doi.org/10.1890/120332.

Tang, H., Song, X.-P., Zhao, F.A., Strahler, A.H., Schaaf, C.L., Goetz, S., Huang, C., Hansen, M.C., Dubayah, R., 2019. Definition and measurement of tree cover: a comparative analysis of field-, LiDAR-, and Landsat-based tree cover estimations in the sierra National Forests, USA. Agric. For. Meteorol. 268, 258–268. https://doi.org/10.1016/j.agrformet.2019.01.024.

Tenneson, K., Patterson, M.S., Mellin, T., Nigrelli, M., Joria, P., Mitchell, B., 2018. Development of a regional LiDAR-derived above-ground biomass model with Bayesian model averaging for use in ponderosa pine and mixed conifer forests in Arizona and New Mexico, USA. Remote Sens. 10 (3), 442. https://doi.org/10.3390/rs10030442.

Timm, B.C., McGarigal, K., Cushman, S.A., Ganey, J.L., 2016. Multi-scale Mexican spotted owl (*Strix occidentalis lucida*) nest/roost habitat selection in Arizona and a comparison with single-scale modeling results. Landsc. Ecol. 31, 1209–1225. https://doi.org/10.1007/s10980-016-0371-0.

U.S. Fish and Wildlife Service, 2012. Mexican Spotted Owl Recovery Plan, First Revision (*Strix occidentalis lucida*). US Fish and Wildlife Service, Southwest Region, Albuquerque, NM. https://www.fs.usda.gov/rm/pubs_other/rmrs_2012_us_fish_wildlife.pdf.

U.S. Forest Service, 2018a. Apache-Sitgreaves National Forests GIS Data. U.S. Department of Agriculture, U.S. Forest Service. https://www.fs.usda.gov/detail/r3/landmanagement/gis/?cid=stelprdb5202663.

U.S. Forest Service, 2018b. Tonto National Forests GIS Data. U.S. Department of Agriculture, U.S. Forest Service. https://www.fs.usda.gov/detail/r3/landmanagement/gis/?cid=stelprdb5209307.

U.S. Geological Survey, 2014. National Elevation Dataset (1999-2013). https://lta.cr.usgs.gov/NED.

Vierling, K.T., Vierling, L.A., Gould, W.A., Martinuzzi, S., Clawges, R.M., 2008. LiDAR: shedding new light on habitat characterization and modeling. Front. Ecol. Environ. 6 (2), 90–98. https://doi.org/10.1890/070001.

Wan, H.Y., McGarigal, K., Ganey, J.L., Lauret, V., Timm, B.C., Cushman, S.A., 2017. Meta-replication reveals nonstationarity in multi-scale habitat selection of Mexican spotted owl. Condor 119 (4), 641–658. https://doi.org/10.1650/CONDOR-17-32.1.

Wan, H.Y., Ganey, J.L., Vojta, C.D., Cushman, S.A., 2018. Managing emerging threats to spotted owls. J. Wildl. Manag. 82, 682–697. https://doi.org/10.1002/jwmg.21423.

Wan, H.Y., Cushman, S.A., Ganey, J.L., 2019a. Improving habitat and connectivity model predictions with multi-scale resource selection functions from two geographic areas. Landsc. Ecol. 34, 503–519. https://doi.org/10.1007/s10980-019-00788-w.

Wan, H.Y., Cushman, S.A., Ganey, J.L., 2019b. Recent and projected future wildfire trends across the ranges of three spotted owl subspecies under climate change. Front. Ecol. Evol. 7, 37. https://doi.org/10.3389/fevo.2019.00037.

Wan, H.Y., Cushman, S.A., Ganey, J.L., 2020. The effect of scale in quantifying fire impacts on species habitats. Fire Ecol. 16 (1), 9. https://doi.org/10.1186/s42408-020-0068-2.

Wing, B.M., Ritchie, M.W., Boston, K., Cohen, W.B., Olsen, M.J., 2015. Individual snag detection using neighborhood attribute filtered airborne lidar data. Remote Sens. Environ. 163, 165–179. https://doi.org/10.1016/j.rse.2015.03.013.